A simple and sensitive electrochemical biosensor for circulating tumor cell determination based on dual-toehold accelerated catalytic hairpin assembly

Xiaohe Zhang[2,3] · Xiujuan Jiang[2,3] · Wen Wang[2,4] · Shihua Luo[2,3] · Shujuan Guan[2,3] · Wenbin Li[2,3] · Bo Situ[2,3] · Bo Li[2,3] · Ye Zhang[2,3] · Lei Zheng[2,3,1] 🅾

Abstract

Tumor cells in blood circulation (CTCs) are vital biomarkers for noninvasive cancer diagnosis. We developed a simple and sensitive electrochemical biosensor based on dual-toehold accelerated catalytic hairpin assembly (DCHA) to distinguish CTCs from blood cells. In the presence of CTCs, the aptamer probe initiates the DCHA process, which produces amplified electrochemical signals. Compared with conventional catalytic hairpin assembly (CHA), the proposed DCHA showed high sensitivity, which led to a broader working range of 10–1000 cells mL^{-1} with a limit of detection of 4 cells mL^{-1}. Furthermore, our method exhibited an excellent capability of distinguishing malignant breast cancers from healthy people, with a sensitivity of 97.4%. In summary, we have established an enzyme-free, easy-to-operate, and nondisruptive method for detecting circulating tumor cells in blood circulation based on the DCHA strategy. Its versatility and simplicity will make it more widely used in clinical diagnosis and biomedical research.

Introduction

Circulating cancer cells (CTCs) are a class of cells that detach from solid tumors and travel in the bloodstream to seed a new tumor in a distant organ. Previous studies have provided evidence that CTCs in peripheral blood are associated with progression, recurrence, survival, and responses to therapy [1, 2]. The analysis of CTCs in cancer has been considered of great value in early diagnosis, metastasis monitoring, and prognosis evaluation [3–5]. However, the rareness of CTCs remains an obstacle to distinguishing them from blood cells [6–8]. Recently, various platforms have been proposed for CTC analysis, such as flow cytometry, fluorescent spectrometry, colorimetry, electrochemilumi-nescence, Raman spectrometry, and electrochemical biosensors [9–16]. Among them, electrochemical biosensors have attracted increasing interest due to their simple operation and wide linear range, which are suitable in clinical settings.

Currently, many efforts have been made in electrochemical biosensor fields for CTC quantification, for example, nanomaterial-based methods, enzyme-assisted strategies, and enzyme-free isothermal amplification [17–19]. As an enzyme-free isothermal amplification method, catalytic hairpin assembly (CHA) is driven by metastable hairpins. It became attractive due to selectivity and simplicity [20–22]. The CHA process only requires two DNA hairpin structures (H1 and H2). In the presence of the initiator probe, the hairpins open and form many DNA duplexes through toehold-mediated strand

Xiaohe Zhang and Xiujuan Jiang contributed equally to this work.

✉ Ye Zhang
zhangye232@i.smu.edu.cn

✉ Lei Zheng
nfyyzhenglei@smu.edu.cn

1 Department of Clinical Laboratory, Shunde Hospital, Southern Medical University, (The First People's Hospital of Shunde), Foshan, 528300 Guangdong Province, China

2 Laboratory Medicine Center, Department of Laboratory Medicine, Nanfang Hospital, Southern Medical University, Guangzhou 510515, China

3 Guangdong Engineering and Technology Research Center for Rapid Diagnostic Biosensors, Nanfang Hospital, Southern Medical University, Guangzhou 510515, China

4 Medical Laboratory of Shenzhen Luohu People's Hospital, Shenzhen 518003, Guangdong Province, China

displacement, leading to amplified signals (Fig. S2). However, the low sensitivity and efficiency were the major issues hindering the clinical application of CHA-related strategies. In this regard, a mismatched CHA strategy was proposed to decrease the nonspecific background signal caused by hairpin breathing [23, 24]. Although the sensitivity increased, the reaction efficiency was also inhibited. A localized CHA strategy has also been proposed to improve the analytical performance of CHA [25]. The CHA reactants were confined on DNA nanowires such that the whole process accelerated in the compact space. However, the locally high concentration of reactants may lead to an unexpected background signal. The relatively low reaction efficiency and sensitivity limit CHA methods used in CTC analysis.

Aptamers are a class of oligonucleotides with high affinity and selectivity to specific target molecules and are considered an alternative to antibodies. Compared with conventional immunoassays using antibodies, aptamer-based methods have a widespread application in detection, diagnosis, and biosensors due to their small size, good biocompatibility, and unique properties [26–30]. Therefore, it is essential to design an appropriate aptamer for CTC recognition and detection.

In this work, we proposed a sensitive, simple, and specific electrochemical biosensor for distinguishing MCF-7 breast cancer cells from blood cells based on a bifunctional aptamer and dual-toehold accelerated catalytic hairpin assembly (DCHA). The DCHA strategy included a hairpin structure containing two toehold domains, which could improve the binding rate of the initiation probe and hairpin. Thus, the sensitivity and efficiency of the subsequent CHA process were greatly increased. Moreover, the bifunctional aptamer probe (Apt probe) consists of a cell-selective domain and a triggered domain. A single-stranded aptamer probe was designed to recognize mucin-1 (MUC1) on MCF-7 cells. Upon selective binding to MUC 1 on MCF-7 cells, the Apt probe exposed the trigger domain that initiated DCHA. The Apt probe hybridized with two toehold regions of H1, which can accelerate the hybridization kinetics of CHA without an unexpected background signal. Through the combination of a bifunctional aptamer and a DCHA amplification strategy, sensitive and efficient CTC detection can be achieved via this developed electrochemical platform. Moreover, owing to the simple sequence design of aptamer probes, it also holds great potential to become a universal detection platform for CTCs.

Experiment section

Reagents and materials

All oligonucleotides used in this work were synthesized by Sangon, Inc. (Shanghai, China), and HPLC-purified.

The detailed sequences are listed in Table S1. TE buffer was acquired from Biosharp (Anhui, China) for dissolving and stocking DNA oligonucleotides. DL500 DNA marker and agarose were purchased from Takara Biotechnology (Dalian, China). All chemicals, including 6-mer-capto-1-hexanol (MCH), streptavidin–alkaline phosphatase (ST-AP), α-naphthyl phosphate (α-NP), and bovine serum albumin (BSA), were obtained from Sigma−Aldrich Inc. (St. Louis, MO, USA). DMEM, RPMI 1640 medium, trypsin, fetal bovine serum, phosphate-buffered saline (PBS), and penicillin−streptomycin were obtained from Thermo Fisher Scientific, Inc. (Shanghai, China). TNaK buffer containing 20 mM Tris–HCl, 125 mM NaCl, and 20 mM KCl (pH 7.4) was used as a hybridization buffer. The binding buffer (pH 7.5) with 10 mM Tris–HCl, 500 mM NaCl, and 1 mM $MgCl_2$ was stored at 4 °C for further use. The red blood cell lysis buffer (pH 7.2–7.4) consisted of 1.5 M NH_4Cl, 100 nM $KHCO_3$, and 1 mM $EDTANa_2$. The washing buffer included Tris–HCl buffer and diethanolamine (DEA) buffer. Tris–HCl buffer consisted of 100 mM NaCl, 20 mM Tris, 5.0 mM $MgCl_2$, and 0.05% Tween-20. DEA buffer consisted of 100 mM DEA, 100 mM KCl, and 1 mM $MgCl_2$. Above all, the reagents were of analytical reagent grade.

Cell culture and preparation

Human breast cancer cell line MCF-7 cells were employed as target cells, while human breast cancer cell line MDA-MB-231 cells, human bronchial epithelial 16HBE cells, and leukocytes were control cells. MCF-7, MDA-MB-231, and 16HBE cells were obtained from the Cell Bank of Type Culture Collection of the Chinese Academy of Sciences (Shanghai, China). MCF-7 and MDA-MB-231 cells were cultured in DMEM, whereas 16HBE cells were cultured in RPMI 1640 medium. The media also contained 10% fetal bovine serum and 1% penicillin−streptomycin and were cultured at 37 ℃ in an atmosphere of 5% CO_2. Cells in the logarithmic growth phase were collected by centrifugation at 1000 rpm for 3 min, followed by discarding the supernatant. Then, the pellet was resuspended in sterile PBS to obtain a homogeneous cell suspension. The number of cells was counted with a Neubauer hemocytometer.

Preparation of DCHA probes

The working hairpins of DCHA were designed according to the theory of the enzyme-free strand displacement reaction. All DNA probes were denatured at 95 °C for 5 min and cooled gradually to room temperature before use. The probes were stored at 4 °C for subsequent CTC detection.

The structures of H1 and H2 are shown in Fig. S1. The parameters of the hairpins, including Gibbs free energy

(DG), enthalpy change (DH), and entropy change (entropy change), were calculated by Oligo Analyzer 3.1 (Integrated DNA Technologies, Skokie, USA) (Table S2). When these values were lower, the secondary structures of H1 and H2 remained constant, indicating reduced background signals during DCHA.

Preparation and measurement of the electrochemical biosensor

The bare gold electrodes should be modified with capture probes before use. The procedures were as follows: first, 0.05 µm alumina powder was used for polishing the gold electrode, followed by removing residual alumina slurries through ultrasonic treatment in deionized water three times. Then, soaking in piranha solution ($H_2SO_4:H_2O_2 = 3:1$) eliminated the organic contaminants on the surfaces thoroughly. After rinsing with ultrapure water and drying with nitrogen, 10 µL thiolated capture probe (prediluted to 200 nM) was dropped onto the prepared electrode surface and incubated overnight at 4 °C. Next, electrodes were immersed into 1 mM MCH solution and 2% BSA sequentially to occupy the nonspecific binding sites on the surface. The gold electrodes were finally ready after cleaning with washing buffer for subsequent detection. A CHI660D electrochemical workstation (Shanghai Chenhua Instrument Co., Ltd., China) was used to collect electrochemical signals.

DCHA detection protocols

First, 10 µL of 100 nM Apt-trigger probes and cell suspensions were added to 1 mL binding buffer. Then, the mixture was incubated at 37 °C for 30 min in a hybridization oven (Scientz LF-III, China) at the appropriate speed. Subsequently, the solution was centrifuged at 2000 rpm for 8 min to obtain the Apt-triggered bound cell sediment.

The Apt probe-bound cell sediment was suspended in 20 µL PBS. Then, the Apt-triggered bound cell suspension was mixed with H1 (250 nM) and H2 (250 nM) in TNaK buffer to 40 µL, which was reacted at 37 °C for 30 min. Then, the solution was centrifuged at 3000 rpm for 3 min to obtain the supernatant. The CHA products were hybridized with the capture probes immobilized on the gold electrode for 30 min. Then, 10 µL of 0.9 µg mL^{-1} ST-AP was dipped onto the electrochemical biosensor at 37 °C for 30 min. Finally, the differential pulse voltammetry (DPV) measurement was performed in DEA buffer containing 1 mg mL^{-1} α-NP substrate, and the experimental parameters were as follows: modulation time of 0.05 s, interval time of 0.017 s, and potential of 0.0 to + 0.6 V.

PAGE electrophoresis

The feasibility of the DCHA strategy was determined by 12% native polyacrylamide gel electrophoresis (PAGE). Twelve percent PAGE was performed in 0.5 × TBE buffer with 140 V constant voltage for approximately 30 min. The gels were stained with 4S Red Plus and scanned by a Bio-Rad electrophoresis analyzer (Bio-Rad, USA).

Fluorescence measurement

The whole volume of the DCHA reaction system was 20µL. The system was diluted to 60µL with DEPC-treated water, and measured fluorescence signal by luminescence spectrometer (PerkinElmer LS-55, USA). The excitation wavelength was 488 nm, and 515 nm was chosen as the emission wavelength.

Pretreatment of clinical samples

Whole blood samples were collected from 10 healthy donors and 20 breast cancer patients (Nanfang Hospital, Southern Medical University) with Nanfang Hospital Ethics approval. One milliliter of 1X red cell lysis solution was mixed with the whole blood samples thoroughly. The mixture was placed at 4℃ until it became completely transparent. After centrifugating at 2200 rpm for 8 min, the pellet was then resuspended in PBS to obtain white cell suspension. The cell suspension was incubated with an aptamer probe and used for subsequent DPV analysis.

Results and discussion

Principle of the DCHA for MCF-7 cell detection

MUC 1 exists on the membrane of epithelial cell types and is highly expressed in various cancers. Aberrantly high expression of MUC1 is associated with tumorigenesis and is considered a promising biomarker for breast cancer [31, 32]. As depicted in Scheme 1, the Apt probe contained a recognition domain for MUC1 and a trigger sequence to activate subsequent DCHA amplification. In the presence of MUC1 on MCF-7 cells, the Apt probe bound to the target and unfolded to expose the trigger sequence to initiate the amplification stage. Then, Apt probes were released by H2 to initiate the next amplification cycles. Therefore, DCHA proceeded promptly and generated large numbers of DNA duplexes modified with biotin molecules. As the DNA duplexes could hybridize with capture probes on the electrode surface, massive biotin molecules were seized for anchoring ST-AP. After incubation with α-NP, ST-AP catalyzed α-NP to generate electrochemical signals, which

Scheme 1 a Bifunctional aptamer probe recognized MUC1 on MCF-7 cells; **b** schematic illustration of the DCHA-based electrochemical platform for detecting MUC1 on MCF-7 cells
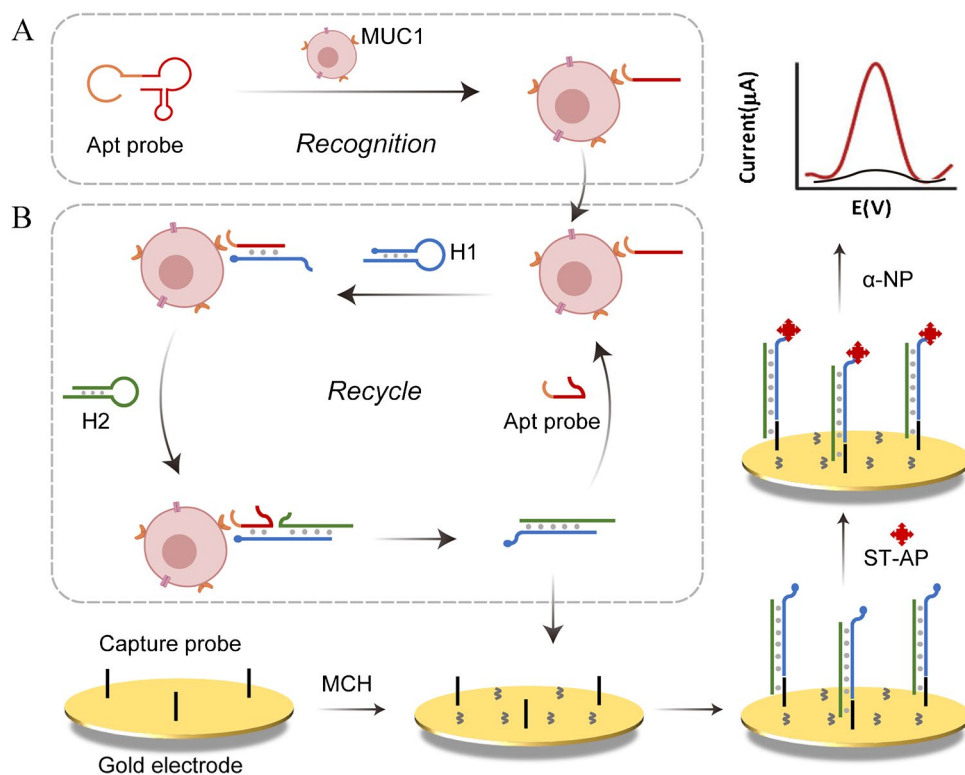
could be used for quantifying MUC1 on MCF-7 cells. The whole DCHA process was the same as the conventional CHA process.

Probe design principle and validation of DCHA

The design of all probes involved in this strategy conformed to the DCHA strategy. As shown in Fig. S2, the conventional structure of H1 in the CHA reaction only contains a single toehold domain [19]. Once the trigger probe hybridized with the toehold, the stem of H1 could be opened and formed stable duplexes with H2. In addition, the toehold located on the loop structure also permits hybridization between H1 and the trigger probe, leading to the formation of H1–H2 duplexes. The whole CHA process was driven by the free-energy hybridization of metastable hairpins. In this work, we introduced two toehold domains on H1, which accelerated hybridization efficiency to overcome the disadvantage of insufficient displacement capability in conventional CHA (Fig. 1A). These two toeholds located on both ends of branch migration domains can increase the binding stability, and the accumulating energy breaks the energy barrier during the displacement process. The opened H1 still exposed enough domain to interact with H2 because the second toehold was only slightly extended. Therefore, the subsequent duplex generation was not affected.

The performance of DCHA was verified by polyacrylamide gel electrophoresis (PAGE). As depicted in Fig. 1B,

the sequences of the Apt probe, H1, and H2 (lanes 1–3) are consistent with our design. In the absence of the Apt probe, H1 and H2 coexisted and showed two independent bands (lane 4), indicating no signal leakage. When the trigger or Apt probe was presented, a new band of CHA or DCHA products was observed, as shown in lanes 5 and 6, respectively. The new band positions are higher, which indicates the successful formation of DNA duplexes. In addition, the band of duplexes generated by DCHA was brighter than that generated by CHA (Fig. 1C), and residual H1 and H2 were barely observed, demonstrating that DCHA proceeds as designed and has higher efficiency.

Next, we demonstrated DCHA efficiency by measuring fluorescent signals. The FAM and quencher were modified at the 5' and 3' ends of H1, respectively. After incubation with the Apt probe for 30 min, the fluorescent signals were measured at 515 nm. DCHA had a more significant fluorescent signal, two times higher than that of conventional CHA (Fig. 1D and E). This result suggested the enhanced reaction efficiency of DCHA, which generated considerable amounts of H1–H2 duplexes.

Characterization of electrode surface modification

The assembly process of DCHA on the electrode surface was characterized by electrochemical impedance spectroscopy (EIS) and square wave voltammetry (SWV). The EIS measurements were performed in 0.4 M KCl containing
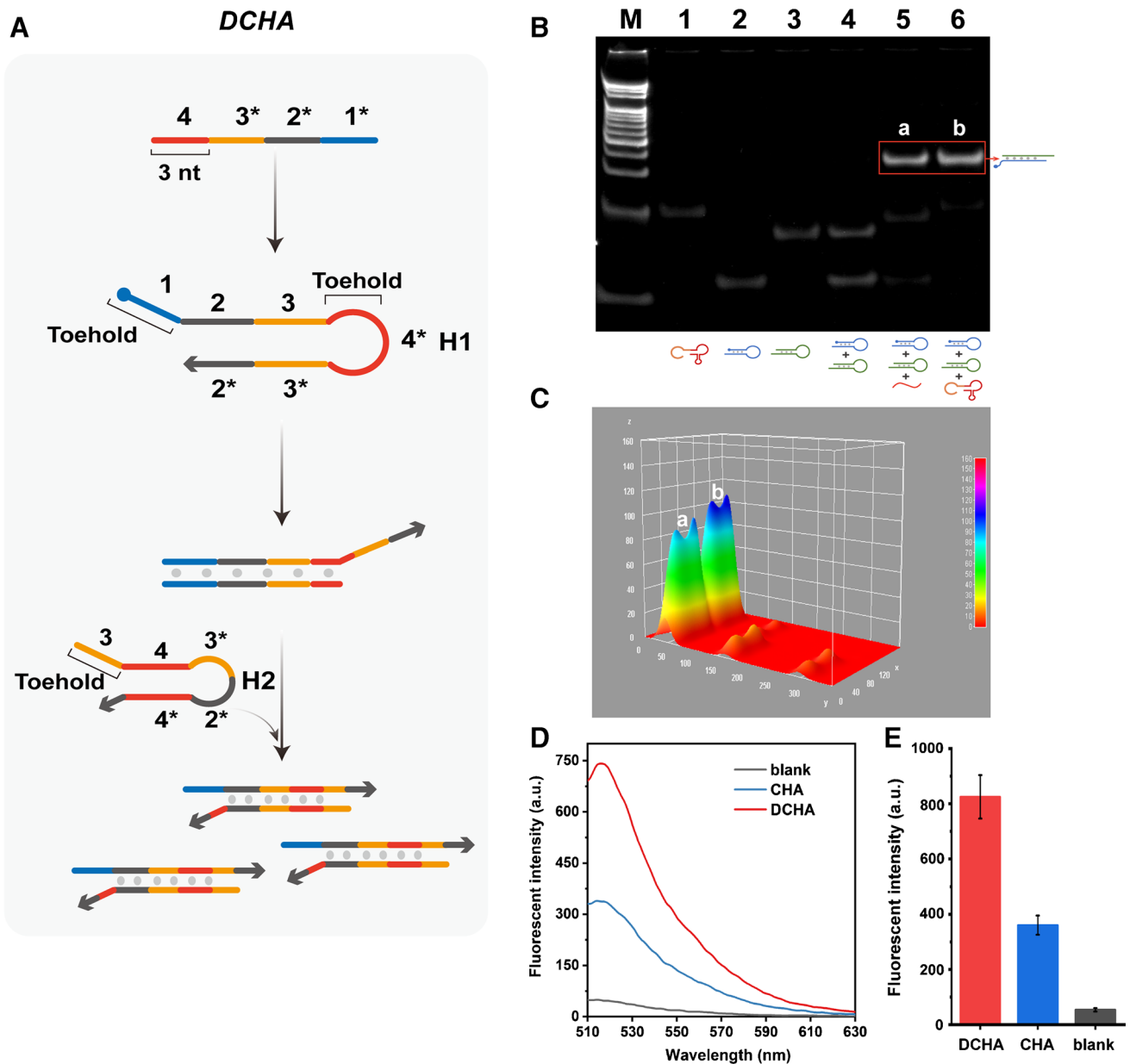
Fig. 1 **A** Schematic representation of the DCHA designed principle. **B** Analysis of DCHA using 12% PAGE and corresponding histogram (**C**). Lane M: 20 bp DNA ladder marker; lane 1: Apt probe; lane 2: H1; lane 3: H2; lane 4: H1+H2; lane 5: H1+H2+trigger; lane 6: H1+H2+Apt probe. Validation of the DCHA performance: **D** fluorescence spectra of conventional CHA (blue curve) and DCHA (red curve), and corresponding histogram (**E**)

0.5 mM $[Fe(CN)_6]^{3-/4-}$, with the open circuit potential over a range of frequency from 0.01 to 10^4 Hz (amplitude: 5 mV). With the alternations of current frequency, the semicircle of the EIS curve represents electron transfer resistance (Ret), which reflects the impedance changes on the electrode. As depicted in Fig. 2A, the bare gold electrode appeared nearly a straight line due to the approachability of $[Fe(CN)_6]^{3-/4-}$ molecules to the surface and prominent electrochemical conductivity (curve a). After incubation with thiolated capture probes, the electrode surface was covered by negatively charged DNA, leading to rejection of the $[Fe(CN)_6]^{3-/4-}$ molecules and a slight increase in Ret (curve b). Then, MCH and BSA were added to the surface to block the residual sites, and the Ret variation became much larger due to the inaccessibility of $[Fe(CN)_6]^{3-/4-}]$ caused by steric hindrance (curves c and d). In the absence of the Apt probe, the EIS curve barely changed with the DCHA system (curve e). With the addition of the Apt probe, the mass of DNA duplexes on the electrode surface shows remarkable negativity; thus,

Fig. 2 EIS (**A**) and SWV (**B**) in 0.4 M KCl containing 0.5 mM [Fe(CN)6]$^{3-/4-}$ at bare electrode (a), capture probe modified electrode (b), MCH and BSA immobilized on the electrode surface (c, d), capture probe modified electrode hybridized with CHA system (e), and with DCHA system (f), respectively
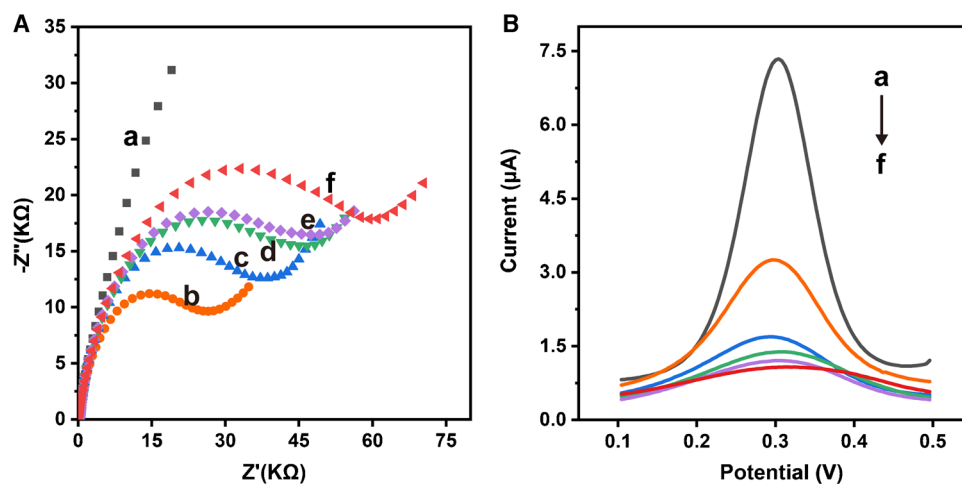
the Ret increased significantly (curve f). The equivalent circuit was used to fit the impedance data (Figure S3). Figure 2B shows the corresponding SWV curves. The changes in peak currents were consistent with the variations in Ret values. By the gradual steps of modification on the electrode surface, the Ret values increased, and the current peaks decreased, indicating successful DCHA formation.

Optimization of detection conditions

To further confirm the superiority of DCHA, we also performed DPV measurements. The superiority of DCHA was also confirmed by the DPV results, which are in good accordance with the fluorescent signals (Figure S4). Several parameters should be investigated to acquire the best analytical performance of this electrochemical biosensor. The DPV peak currents and signal-to-noise (S/N) were used to evaluate the optimization effects. The rational design of the second toehold length is a prerequisite to minimizing affecting factors in the displacement process. We designed several sequences with different lengths of the second toehold domain (Table S3). As shown in Fig. S5A, the DPV peak current increases with increasing base numbers of the second toehold domain from 0 to 3. However, as the number of bases increases from 4 to 5, the DPV peak current begins to decrease. Excess base numbers of the second toehold domain result in reduced hybridization efficiency, possibly because the stable intermediate H1-Apt duplexes influence the subsequent strand displacement process. Thus, a length of 3 bases in the second toehold domain is used in subsequent experiments. We also compared the differences in DPV and S/N under different reaction times and temperatures. The optimized conditions were 37 °C as the reaction temperature and 30 min as the appropriate incubation time (Fig. S5B and C).

Analytical performance of the developed electrochemical biosensor

Under these optimized experimental conditions, the analytical performance of the electrochemical biosensor for MCF-7 cell detection was studied. We applied MCF-7 cells at concentrations ranging from 10 to 10^5 cells/mL to verify sensitivity. The DPV current gradually increased with the concentration of MCF-7 cells, indicating the excellent response of DCHA to MCF-7 cells (Fig. 3A). A good correlation between the DPV peak current and the logarithm of the MCF-7 cell number was verified. The linear range of 10 ~ 1000 cells/mL was obtained by the equation $y = 0.215 \pm 0.012\log_{10}C + 0.831$, in which y represents the DPV peak current and C represents the cell concentration (Fig. 3B). The limit of detection (LOD) was calculated to be 4 cells/mL by three standard deviations, enabling recognition of CTCs in clinical samples. Compared with previous CTC analysis methods, the developed electrochemical biosensor exhibited the advantages of being sensitive, efficient, and simple (Table S4). The capacity to accurately differentiate MCF-7 cells from blood cells is also essential for clinical application. We then used four types of cells with different MUC-1 expression levels, including MDA-MB-231 cells, 16HBE cells, leukocytes, and mixed cells (16HBE and MCF-7, 1:1 mixed), as control groups to verify the selectivity of the DCHA strategy-based electrochemical biosensor. As illustrated in Fig. 3C, the DPV currents of leukocytes and 16HBE cells were almost the same as those of the blank group. The DPV currents from MCF-7 cells were approximately fivefold higher than MDA-MB-231 cells, which was consistent in other reported works of literature that MDA-MB-231 cells had correspondingly low MUC-1 expression levels. There was a great correlation between DPV signals and MUC-1 expression levels. And the mixed cells showed similar DPV currents as the MCF-7 cells, indicating the excellent selectivity of the DCHA strategy for MUC-1 on
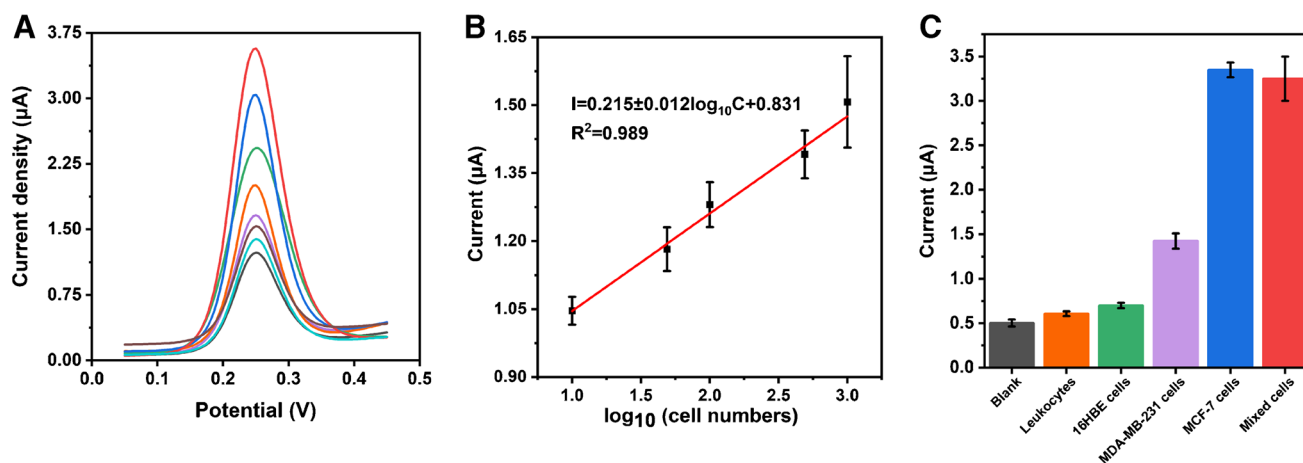
Fig. 3 Analytical performance of the DCHA-based electrochemical biosensor: **A** DPV responses and **B** the corresponding correlation linear curve for 100,000, 50,000, 10,000, 1000, 500, 100, 50, 10 cells mL^{-1} MCF-7 cells. **C** Selectivity assessment in different cell lines. Mixed cells: the mixture of MCF-7 and 16HBE cells at a ratio of 1:1

the cytomembrane. Meanwhile, the stability of this biosensor had been assessed with DPV measurement every other day. As shown in Fig. S6, the DPV signal basically remained more than 85% of the initial signal value during 7 days. The samples containing 500 and 10^4 cells were tested for intra-batch and inter-batch precision. The coefficient of variation was about 6.3% (Fig. S7), which demonstrated this biosensor had acceptable reproducibility. Taken together, the proposed electrochemical biosensor is a promising tool for clinical CTC analysis.

Evaluation of analytical performance in clinical samples

We next assessed the clinical application of the proposed biosensor. Considering the complex matrix of clinical specimens, we randomly collected plasma from clinical patients. Then, different numbers of MCF-7 cells (10^2, 10^3, 10^4, and 10^5) were added to the collected plasma. We used this biosensor to measure the DPV signals of MCF-7 cells in different matrices. The differences in signal could be observed between whole blood and buffer in the 10^2 and 10^3 cell number groups. CTCs in whole blood were surrounded by abundant cells, such as leukocytes and erythrocytes, which might impede the initiation of DCHA. The relatively poor efficiency of DCHA in whole blood made the signal lower than the PBS group. There were negligible changes in DPV signals between PBS buffer and plasma when the numbers of MCF-7 cells were 10^4 and 10^5 mL (Fig. 4A), suggesting that the proposed biosensor can determine CTCs even in a complex environment.

Moreover, the DCHA-based electrochemical biosensor was used for CTC analysis in clinical whole blood specimens. We studied breast cancer patients (BC, $n = 20$) and

compared them with healthy donors (HD, $n = 10$). After measurement by the biosensor, the electrochemical signals are shown in Fig. 4B and C. The DPV currents between the two groups differed greatly. There was a significant increase in CTCs in the blood of breast cancer patients ($p < 0.001$) compared with healthy donors. The concentration of CTCs in the BC groups was higher than 10 cells/mL, and that in the HD groups was approximately 5 cells/mL. The quantitative results could be used to distinguish the BC groups from HD, which was consistent with the clinical diagnosis data (Table S5). The CTC analysis showed an area under the curve (AUC) of 0.955 (95% CI: 0.9430–1.0000) with a sensitivity of 85% and a specificity of 100% (Fig. 4D). As shown in Fig. S8, the results obtained from DCHA were identical with clinical CTC results. Therefore, the electrochemical biosensor might satisfy the urgent need for CTC analysis in clinical settings.

Conclusions

In this work, we proposed an innovative electrochemical biosensor for CTC analysis that is simple and sensitive and does not require tedious equipment. The designed DCHA strategy improved the efficiency and sensitivity by increasing the hybridization-driven free energy. The DCHA-based electrochemical biosensor had a detection limit of 4 cells mL^{-1} with simple operation and low cost. Meanwhile, this biosensor also holds great potential to work in a complex environment and for practical applications, and it can distinguish CTCs from the blood samples of patients with an AUC of 0.955. However, there is still a need for large-scale clinical sample verification if this platform is used for clinical applications. Another challenge to be solved is how

Fig. 4 Analytical performance of this biosensor in clinical samples. **A** Detecting MCF-7 cells in buffer and whole blood. Error bars represent the standard deviation in three different measurements at each concentration. **B** Electrochemical bar graph of clinical samples (10 healthy donors (HD) and 20 breast cancer patients (BC)) measured by the DCHA-based electrochemical biosensor. **C** Scatter plot of clinical experiment according to the data from Fig. 4A, MUC-1 positive cells were elevated in BR compared to HD (***, $p < 0.001$). **D** ROC curve of CTCs measured by this platform for distinguishing BC from HD
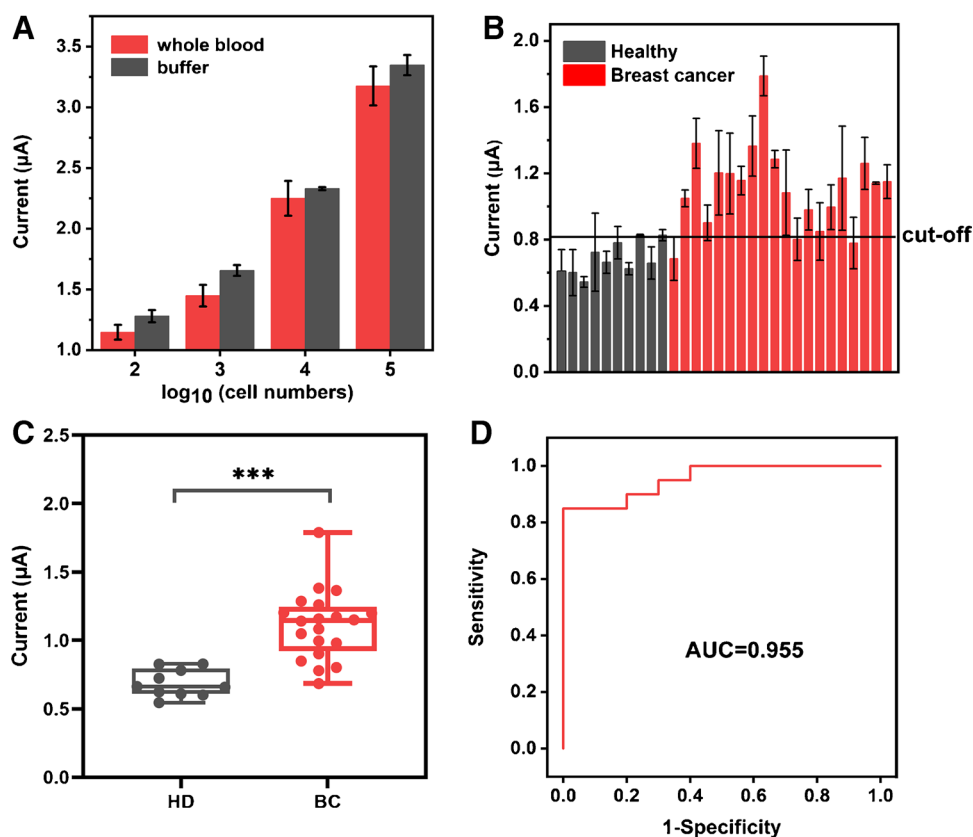
to remove the contaminants from plasma and exosomes. The pretreatment of clinical samples in this work used red cell lysis solution to selectively lyse the erythrocytes, and isolated leukocytes and CTCs from the whole blood. After removing the cell debris through centrifugation, there were only a few exosomes remaining in the supernatant. The effect of the remaining exosomes on the signal could be negligible. In summary, this electrochemical biosensor is expected to become a new clinical tool with great development prospects for early cancer diagnosis and prognosis monitoring.

Declarations

Competing interests The authors declare no competing interests.

References

1. Bidard FC, Peeters DJ, Fehm T, Nole F, Gisbert-Criado R, Mavroudis D et al (2014) Clinical validity of circulating tumour cells in patients with metastatic breast cancer: a pooled analysis of individual patient data. Lancet Oncol 15(4):406–414. https://doi.org/10.1016/S1470-2045(14)70069-5

2. Li W, Wang H, Zhao Z, Gao H, Liu C, Zhu L et al (2018) Emerging nanotechnologies for liquid biopsy: the detection of circulating tumor cells and extracellular vesicles. Adv Mater 31(45):1805344. https://doi.org/10.1002/adma.201805344

3. Husemann Y, Geigl JB, Schubert F, Musiani P, Meyer M, Burghart E et al (2008) Systemic spread is an early step in breast cancer. Cancer Cell 13(1):58–68. https://doi.org/10.1016/j.ccr.2007.12.003

4. Allard WJ, Matera J, Miller MC, Repollet M, Connelly MC, Rao C et al (2004) Tumor cells circulate in the peripheral blood of all major carcinomas but not in healthy subjects or patients with nonmalignant diseases. Clin Cancer Res 10(20):6897–6904. https://doi.org/10.1158/1078-0432.CCR-04-0378

5. Mohammed I, Oluwole DO, Nemakal M et al (2019) Investigation of novel substituted zinc and aluminium phthalocyanines for

photodynamic therapy of epithelial breast cancer. Dyes and Pigments 170:107592. https://doi.org/10.1016/j.dyepig.2019.107592

6. Lin E, Cao T, Nagrath S, King MR (2018) Circulating tumor cells: diagnostic and therapeutic applications. Annu Rev Biomed Eng 20:329–352. https://doi.org/10.1146/annurev-bioeng-062117-120947

7. Song P, Ye D, Zuo X, Li J, Wang J, Liu H et al (2017) DNA hydrogel with aptamer-toehold-based recognition, cloaking, and decloaking of circulating tumor cells for live cell analysis. Nano Lett 17(9):5193–5198. https://doi.org/10.1021/acs.nanolett.7b01006

8. Pantel K, Alix-Panabières C (2019) Liquid biopsy and minimal residual disease - latest advances and implications for cure. Nat Rev Clin Oncol 16(7):409–424. https://doi.org/10.1038/s41571-019-0187-3

9. Zheng S, Lin HK, Lu B, Williams A, Datar R, Cote RJ et al (2011) 3D microfilter device for viable circulating tumor cell (CTC) enrichment from blood. Biomed Microdevices 13(1):203–213. https://doi.org/10.1007/s10544-010-9485-3

10. Shan Q, Lou X, Xiao T, Zhang J, Sun H, Gao Y et al (2013) A cancer/testis antigen microarray to screen autoantibody biomarkers of non-small cell lung cancer. Cancer Lett 328(1):160–167. https://doi.org/10.1016/j.canlet.2012.08.019

11. Zhang H, Wang Y, Li Q, Zhang F, Tang B (2014) A size amplified immune magnetic microbeads strategy in the rapid detection of circulating tumor cells. Chem Commun 50(53):7024–7027. https://doi.org/10.1039/C4CC02342K

12. Georgakoudi I, Solban N, Novak J, Rice WL, Wei X, Hasan T et al (2004) In vivo flow cytometry: a new method for enumerating circulating cancer cells. Cancer Res 64(15):5044–5047. https://doi.org/10.1158/0008-5472.CAN-04-1058

13. Tang S, Shen H, Hao Y, Huang Z, Tao Y, Peng Y et al (2018) A novel cytosensor based on Pt@Ag nanoflowers and AuNPs/acetylene black for ultrasensitive and highly specific detection of circulating tumor cells. Biosens Bioelectron 104:72–78. https://doi.org/10.1016/j.bios.2018.01.001

14. Cai S, Li G, Zhang X, Xia Y, Chen M, Wu D et al (2015) A signal-on fluorescent aptasensor based on single-stranded DNA-sensitized luminescence of terbium (III) for label-free detection of breast cancer cells. Talanta 138:225–230. https://doi.org/10.1016/j.talanta.2015.02.056

15. Ge S, Zhao J, Wang S, Lan F, Yan M, Yu J (2018) Ultrasensitive electrochemiluminescence assay of tumor cells and evaluation of H2O2 on a paper-based closed-bipolar electrode by in-situ hybridization chain reaction amplification. Biosens Bioelectron 102:411–417. https://doi.org/10.1016/j.bios.2017.11.055

16. Cialla-May D, Zheng XS, Weber K, Popp J (2017) Recent progress in surface-enhanced Raman spectroscopy for biological and biomedical applications: from cells to clinics. Chem Soc Rev 46(13):3945–3961. https://doi.org/10.1039/c7cs00172j

17. Zhu C, Yang G, Li H, Du D, Lin Y, Lab PNN, PNNL R W U S (2015) Electrochemical sensors and biosensors based on nanomaterials and nanostructures. Anal Chem 87(1):230–249. https://doi.org/10.1021/ac5039863

18. Das P, Das M, Chinnadayyala SR, Singha IM, Goswami P (2016) Recent advances on developing 3rd generation enzyme electrode for biosensor applications. Biosens Bioelectron 79:386–397. https://doi.org/10.1016/j.bios.2015.12.055

19. Zheng T, Zhang Q, Feng S, Zhu J, Wang Q, Wang H (2014) Robust nonenzymatic hybrid nanoelectrocatalysts for signal amplification toward ultrasensitive electrochemical cytosensing. J Am Chem Soc 136(6):2288–2291. https://doi.org/10.1021/ja500169y

20. Yin P, Choi HMT, Calvert CR, Pierce NA (2008) Programming biomolecular self-assembly pathways. Nature 451(7176):318–322. https://doi.org/10.1038/nature06451

21. Zhao Y, Chen F, Li Q, Wang L, Fan C (2015) Isothermal amplification of nucleic acids. Chem Rev 115(22):12491–12545. https://doi.org/10.1021/acs.chemrev.5b00428

22. Yang T, Fang J, Guo Y, Sheng S, Pu Q, Zhang L et al (2019) Fluorometric determination of microRNA by using an entropy-driven three-dimensional DNA walking machine based on a catalytic hairpin assembly reaction on polystyrene microspheres. Microchim Acta 186(8):574. https://doi.org/10.1007/s00604-019-3689-x

23. Chen J, Wu Y, Fu C, Cao H, Tan X, Shi W et al (2019) Ratiometric SERS biosensor for sensitive and reproducible detection of microRNA based on mismatched catalytic hairpin assembly. Biosens Bioelectron 143:111619. https://doi.org/10.1016/j.bios.2019.111619

24. Zhang Y, Yan Y, Chen W, Cheng W, Li S, Ding X et al (2015) A simple electrochemical biosensor for highly sensitive and specific detection of microRNA based on mismatched catalytic hairpin assembly. Biosens Bioelectron 68:343–349. https://doi.org/10.1016/j.bios.2015.01.026

25. Wei Q, Huang J, Li J, Wang J, Yang X, Liu J et al (2018) A DNA nanowire based localized catalytic hairpin assembly reaction for microRNA imaging in live cells. Chem Sci 9(40):7802–7808. https://doi.org/10.1039/c8sc02943a

26. Xiang J, Pi X, Chen X, Xiang L, Yang M, Ren H et al (2017) Integrated signal probe based aptasensor for dual-analyte detection. Biosens Bioelectron 96:268–274. https://doi.org/10.1016/j.bios.2017.04.039

27. Li Y, Zhang Y, Zhao M, Zhou Q, Wang L, Wang H et al (2016) A simple aptamer-functionalized gold nanorods based biosensor for the sensitive detection of MCF-7 breast cancer cells. Chem Commun (Camb) 52(20):3959–3961. https://doi.org/10.1039/C6CC01014H

28. Phillips JA, Lopez-Colon D, Zhu Z, Xu Y, Tan W (2008) Applications of aptamers in cancer cell biology. Anal Chim Acta 621(2):101–108. https://doi.org/10.1016/j.aca.2008.05.031

29. Sun D, Lu J, Zhang L, Chen Z (2019) Aptamer-based electrochemical cytosensors for tumor cell detection in cancer diagnosis: a review. Anal Chim Acta 1082:1–17. https://doi.org/10.1016/j.aca.2019.07.054

30. Liu J, Zhang Y, Zhao Q, Situ B, Zhao J, Luo S et al (2018) Bifunctional aptamer-mediated catalytic hairpin assembly for the sensitive and homogenous detection of rare cancer cells. Anal Chim Acta 1029:58–64. https://doi.org/10.1016/j.aca.2018.04.068

31. Kretschmer C, Sterner-Kock A, Siedentopf F, Schoenegg W, Schlag PM, Kemmner W (2011) Identification of early molecular markers for breast cancer. Mol Cancer 10(1):15. https://doi.org/10.1186/1476-4598-10-15

32. Donepudi MS, Kondapalli K, Amos SJ, Venkanteshan P (2014) Breast cancer statistics and markers. J Cancer Res Ther 10(3):506–511. https://doi.org/10.4103/0973-1482.137927